Journal of Photochemistry and Photobiology A: Chemistry 221 (2011) 261–267

Contents lists available at ScienceDirect

Journal of Photochemistry and Photobiology A: Chemistry

journal homepage: www.elsevier.com/locate/jphotochem

Sensitive bioimaging in microfluidic channels on the plasmonic substrate: Application of an enhanced fluorescence based on the reverse coupling mode

Keiko Tawa [a,*], Xiaoqiang Cui [a], Kenji Kintaka [b], Junji Nishii [c], Kenichi Morigaki [a]

[a] Health Research Institute, AIST, Ikeda, Osaka 563-8577, Japan
[b] Photonics Research Institute, AIST, Tsukuba 305-8568, Japan
[c] Research Institute for Electronic Science, Hokkaido University, Hokkaido 001-0021, Japan

ARTICLE INFO

Article history:
Available online 15 April 2011

Keywords:
Fluorescence enhancement
Plasmonic
Reverse coupling
Bioimaging
Nanohole array
Microfluidic channels

ABSTRACT

Grating-coupled surface plasmon-field enhanced fluorescence (GC-SPF) was applied to biosensing. Although the greatest enhancement of GC-SPF on our plasmonic chips compared with that on a glass slide was found to be 40 times, this was due to the enhanced excitation field. Therefore, grating-coupled fluorescence using a reverse coupling mode is here explored to achieve further 4–5 times enhancement. As a result of using both the excitation field enhanced by grating-coupled surface plasmon resonance and the directional emission enhanced by reverse coupling mode, an increase in fluorescence of more than 110 times compared with that on the glass slide was recorded. The reverse coupling mode was also applied to the sensitive fluorescence microscopic imaging of Cy5-streptavidin (Cy5-SA) in microfluidic channels on a two dimensional nanohole array substrate. We performed a Cy5-SA concentration series analysis in which the plasmonic substrate demonstrated 26.3× enhancement of sensitivity and a limit of detection (LOD) of *ca.* 100 pM, which is at least one order of magnitude lower than in glass slides with identical surface chemistry. This plasmonic nanostructure will be invaluable for colorimetric detection in applications such as microfluidic enzyme-linked immune-sorbent assay (ELISA) device, and portable microarray biosensing, because the optical setup can be simplified.

1. Introduction

In grating-coupled surface plasmon resonance (GC-SPR), which is known to be a kind of propagated plasmons, the incident light is introduced to the interface by trapping using a metallic periodic structure instead of a prism [1–5]. The advantage of GC-SPR is that the resonance angle can be controlled by the pitch of the grating. On the other hand, in the Kretschmann configuration of prism-coupled surface plasmon resonance (PC-SPR), even if a prism with high refractive index (e.g. 1.85) and light with a longer wavelength (e.g. 633 nm) could be used, the resonance angle would be above 60° for the water interface [6,7]. The application of PC-surface plasmon-field enhanced fluorescence (SPF) to bio-sensing is complex in operating and constructing optical stuffs for illumination and difficult in using a fluorescence microscope. The lower incident angle in GC-SPR without prism facilitates operation and simplifies the optical setup. Bio-sensors using the fluorescence excited by the enhanced electric fields of GC-SPR, which is known as grating-coupled surface plasmon-field enhanced fluorescence (GC-SPF), are being developed as an application and a number of relevant reports have already been published [8–10]. We have applied GC-SPF specifically to fluorescence microscopic imaging and biosensor-based fluorescence detection [11–14]. In the former application, fluorescence images of cells were more than 20 times enhanced compared with images taken on glass slides [11]. In the latter application, 40 times enhanced fluorescence was detected in a biochip with an optimized grating structure in which the pitch, groove depth, and duty ratio (ratio of convex part) after silver coating were 400 nm, 20 nm, and 0.5, respectively; the surface profile was trapezoid [12–14].

Meanwhile, the reverse coupling mode recently described with the term surface plasmon-coupled emission (SPCE) has been studied in the reverse Kretschmann configuration of PC-SPR [9,15–17]. Fluorescence from molecules may excite SPP modes at the fluorescent dye/metal interface, and these SPP modes may in turn decay to produce light in the prism. Such an SPCE technique has been performed on many structures but seldom on a grating structure. Chiu et al. [9] studied the effect of the reverse coupling mode on the active emission of a grating with organic semiconductor material, Alq_3, on the surface. Feng et al. [18] also reported highly directional emission by GC-SPR tunneling from electroluminescence in organic light-emitting devices. In the present study, on the other hand, the application of the reverse coupling mode to the emission from fluorescent dye-labeled proteins was investigated in biochips with

* Corresponding author. Tel.: +81 72 751 9243.
E-mail address: tawa-keiko@aist.go.jp (K. Tawa).

1010-6030/$ – see front matter © 2011 Elsevier B.V. All rights reserved.
doi:10.1016/j.jphotochem.2011.04.012

silver-coated grating, i.e., in plasmonic chips. The use of reverse coupling mode can simply make the bio-sensing in the lower target concentration possible. We found that the use of the both the enhanced excitation field produced by SPP resonance and the directional emission from the reverse coupling mode provided a very significant fluorescence enhancement in the biochip. Therefore, the reverse coupling mode can be applied to fluorescence microscopic imaging in microfluidics channels.

Microfluidic lab-on-chip devices and micro-total-analysis systems have been widely investigated to advance and simplify complex biosensing applications on small chips [19,20]. In the microfluidic nanohole array, proteins and DNA were sensitively detected by the enhanced surface plasmon resonance signals without fluorescent probe [21,22]. However, the sensitivity is not superior to the fluorescence methods. In colorimetric measurement, which is one of the most popular detection methods using microfluidics techniques [23], fluorescence-based imaging detection has produced detection limits comparable to those of enzyme-linked immune-sorbent assay (ELISA) [24–26]. In this study, fluorescent-labeled marker proteins were detected in the flow system with microfluidic channel device, differing from the sink system used in our previous studies [14]. Flow system makes an evaluation of affinity possible in a bioassay and is a useful technique. The combination of microscope, microfluidic channel, and plasmonic chip achieved highly sensitive fluorescence detection under an easy operation and a simple setup. Various optically passive substrates, such as glass [27], plastic [28,29], PDMS [25,30], and UV-curable epoxy resin [31], have been used in microfluidic devices. Chemical modification of the surfaces is one way to improve the performance of these biosensing devices by eliminating non-specific binding while enhancing biological activity and stability [32,33]. Enhancing the fluorescence of the fluorophores near the surface has proved to be another effective way of improving the performance of fluorescence biosensing systems [34]. For example, photonic crystal surfaces consisting of periodic TiO_2 have been used to enhance the fluorescence detection of protein microarrays [35]. By evaluating the bioassay in a concentration series on plasmonic and glass substrates, we demonstrated the successful application of these plasmonic substrates in a microfluidic channel device.

2. Experimental

2.1. Grating substrate

Grating structures were constructed on two sheets of SiO_2 substrates using a previously reported two-laser-beam interference method followed by dry etching [36]. Briefly, the photoresist pattern was formed by exposing to the interference beam of a He–Cd laser (Kimmon Electric, 1K3501R-G) with 325 nm wavelength, after which the SiO_2 surface was etched by dry etching (ULVAC, NLD-500). The two dimensional (2D) substrate was also fabricated in two identical exposure steps, the substrate being rotated by a 90° angle approximately normal to its surface between exposures. The residual photoresist was then removed by acetone washing and then oxygen plasma treatment. (Yamato, RFG-500A). The slide glass plates (used for control experiment) and grating substrates were cleaned by sonicating in a 1% Hellmanex (Hellma, Müllheim, Germany) solution and rinsing extensively with fresh Milli-Q water, after which they were dried completely under air flow. The fabricated 1D gratings and 2D grating were measured by scanning probe microscopy (SPM). The pitches of the two 1D substrates were 402 and 410 nm (error in measurement by SPM: ±10 nm), the groove depths were found to be 25, and 22 nm (error in SPM measurement: ±3 nm), while the duty ratios before coating (ratio of convex part to the pitch) differed, being 0.71 and 0.56 (error in SPM measurement: ±0.03), for gratings Nos. 1 and 2, respectively. The pitch of the 2D nanohole array was 400 ± 10 nm, the groove depth and the duty ratio were 31 ± 3 nm and 0.33 ± 0.03.

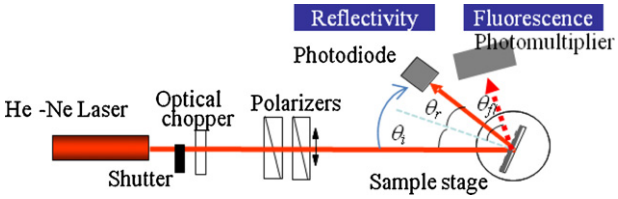

Fig. 1. SPR-SPFS setup.

Thin metal layers covered with a SiO_2 overlayer (with an adhesion layer of Cr) were prepared on both substrates via the following process. First, a Cr layer of less than 1 nm thickness was deposited using an rf sputter setup (Rikensya, specially made) in an Ar gas flow. A 100-nm-thick silver layer and 200-nm-thick silver layer was then deposited on the Cr layer and another Cr layer was deposited for 1D and 2D substrates, respectively, without opening the chamber. Finally, a 20-nm thick SiO_2 layer was deposited on the Cr layer for both substrates. A 20-nm thick SiO_2 layer efficiently suppresses (quenches) energy transfer to the metal layer from the fluorescence excited by the GC-SPR field [8].

The coated substrates were modified with 3-aminopropyltriethoxysilane (APTES, Sigma–Aldrich) aqueous solution (1 vol.%) for 1 h. After reaction, the APTES solution was removed and the substrates rinsed by immersion in Milli-Q water (18.2 MΩ) and ethanol and dried. For detection of labeled proteins, biotin-poly(ethylene glycol)-carbonate-NHS ester [NOF SUNBRIGHT BI-050TS] prepared in aqueous solution (2 mM) was poured onto the surface of the substrates, which were rinsed with Milli-Q water at 1 h after the reaction between the NHS group and the amino group of the substrate surface.

2.2. Reflectivity and fluorescence measurement

A He–Ne laser beam of 632.8 nm wavelength passes through an optical chopper (used also as the reference for the lock-in amplifier) and two polarizers for intensity and polarization control as shown in Fig. 1. Using a $\theta - 2\theta$ goniometer, the light reflected at the substrate is monitored against the incident angle (θ_i) with a photodiode automatically rotating at $\theta_i + \theta_r$ ($\theta_i = \theta_r$). The emission [after passing through a narrow band interference filter, $\lambda = 670 \pm 5$ nm, and notch filter (stopline, Semlock, USA)] is monitored with a photomultiplier mounted on the goniometer stage in the following two ways: incident angle (θ_i)-scanning fluorescence measurement with a photomultiplier fixed at 55° for the incident beam-line; and θ_{fl}-scanning fluorescence measurement under the fixed incident angle θ_i of resonance angle, 30° and 45°. In the fluorescence detection under a chip rotation for axis normal to surface, non-polarized light was incident using a depolarizer.

2.3. Samples

A labeled protein [streptavidin (SA) labeled with Cy5 (Amersham)] was prepared at a concentration of 100 nM with phosphate buffered saline solution for measurement of angle-scanning reflectivity and fluorescence intensity. In order to precisely evaluate the fluorescence enhancement factor on the plasmonic chip compared with the fluorescence intensity measured on the glass slide, the concentration of Cy5-SA of 100 nM was appropriate, because the fluorescence intensity was not precisely measured on the glass slides for 10 nM-Cy5-SA. A cover glass was attached to the top of all substrates and a 20 μL solution was injected into the substrate by

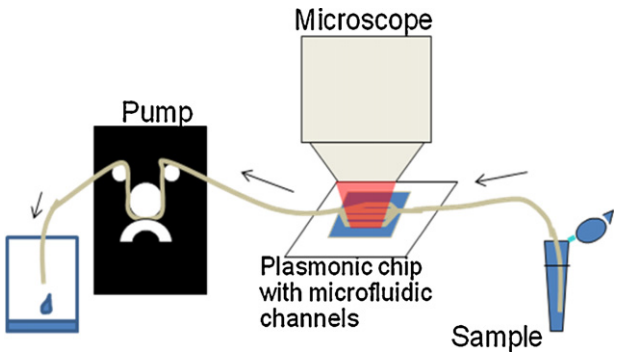

Fig. 2. Microfluidic apparatus under the microscope.

pipette. After thorough rinsing, the proteins were homogeneously bound to the surface of the substrates. Under the fluorescence microscopic imaging of Cy5-SA, the concentration was prepared from 1 μM to 100 pM.

2.4. Fluorescence imaging with microfluidic channels

A PDMS microfluidic microchip with four parallel channels each ~60 μm wide was formed by casting and curing PDMS against a patterned master on a silicon wafer. The PDMS channels were placed in conformal contact with a plasmonic/or glass substrate and each channel was filled with Cy5-SA solutions in PBS using the channel outgas technique. The concentration of Cy5-SA ranged from 100 pM to 1 μM. After incubation for 30 min, the channels were rinsed for 5 min with PBS and then observed under a fluorescence microscope as shown in Fig. 2.

Fluorescence images of microfluidic channels were collected using an upright microscope (BX51WI, Olympus, Tokyo, Japan). The sample was illuminated with an Hg lamp using a Cy5 filter and the fluorescence images were recorded using a CCD camera (Andor Technology, iXon^{EM}+, Ireland) with a 10× objective lens (numerical aperture (NA) = 0.3). During the series of measurements, the illumination intensity, exposure time = 0.03 s, and CCD camera EM gain were all kept constant.

3. Results and discussion

3.1. GC-SPR and GC-SPF

The resonance angles for 1D plasmonic chips Nos. 1 and 2 were detected at 8° and 6°, respectively, at the aqueous solution interface (see references [12–14]). The coupling condition actually depends on the surface profile including duty ratio, and therefore, the different resonance angles were found in Nos. 1 and 2 chips with different structure. Fig. 3(a) points out the resonance angle at the air and water interfaces for No. 2 plasmonic chip. They were almost consistent with the resonance angles deduced from the dispersion relationship with consideration of SiO_2 overlayer as shown in Table 1.

Table 1
Resonance angles and reverse coupling angles.

	Resonance angle (°)	Reverse coupling (°)	
		+	–
No. 1	8	13	15
No. 2	6	10	14
Dispersion relationship	5	13	13

Fig. 3(b) shows the result of the θ_i-dependent fluorescence measurement for No. 2 plasmonic chip. The background signal before injection of Cy5-SA was 2-order smaller than the fluorescence peak value, 1500 ± 500 counts per seconds (cps). The fluorescence peak was also observed at 6° and coincident with the resonance angles and the enhanced fluorescence was therefore considered to be the result of excitation by the enhanced electric fields of GC-SPR. The fluorescence intensity was 3500 ± 1000 cps for labeled protein bound to a biotinylated glass slide without grating (data not shown) and therefore the enhancement factor was 30 times, which shows good agreement with our previous results [12].

3.2. Reverse coupling mode

As shown in Fig. 4, the θ_{fl}-scanning fluorescence was measured at two kinds of fixed incident angles, θ_i = 30° and 45°, for No. 2 1D plasmonic chip. The most enhanced fluorescence peaks were observed at θ_{fl} of 10° and −14° as the detection angle for the substrate normal. As shown in Fig. 4, the curves with double peak corresponding to the + and – reverse coupling angles were not symmetric for 0° of the θ_{fl}. This may be due to the deviation of 0° in the θ_{fl} under the optical arrangement, the deviation of the rotational angle, ψ, and the slight shift of laser illumination spot depending on ψ. The reverse coupling angles for both chips are summarized in Table 1.

The resonance angles and reverse coupling angles obtained from measurements were close to, but not completely consistent with, the values estimated from the dispersion relationship, 5° and 13°. Their deviations within 3° were considered to be due to differences in the uniformity of the pattern and the surface profile of the pattern, including the duty ratio and the groove depth.

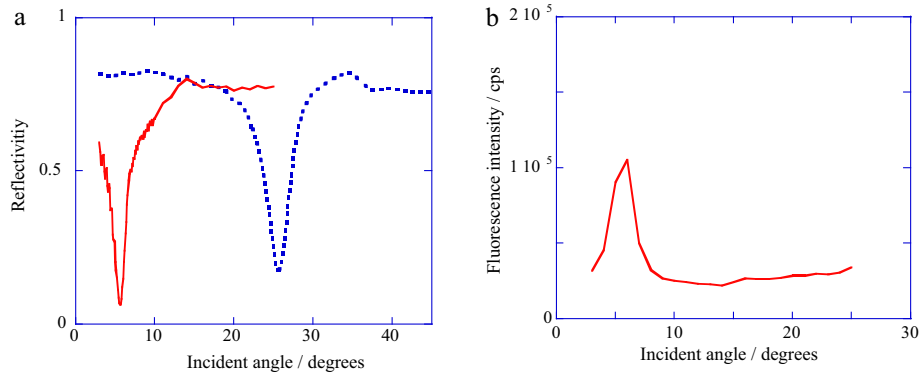

Fig. 3. (a) Curve of reflectivity against incident angle: red solid and blue dot curves correspond to interfaces in water and in air, respectively. (b) Curve of fluorescence intensity against incident angle on the grating No. 2. Fluorescence was detected with a photomultiplier fixed at 55°. (For interpretation of the references to color in this figure legend, the reader is referred to the web version of this article.)

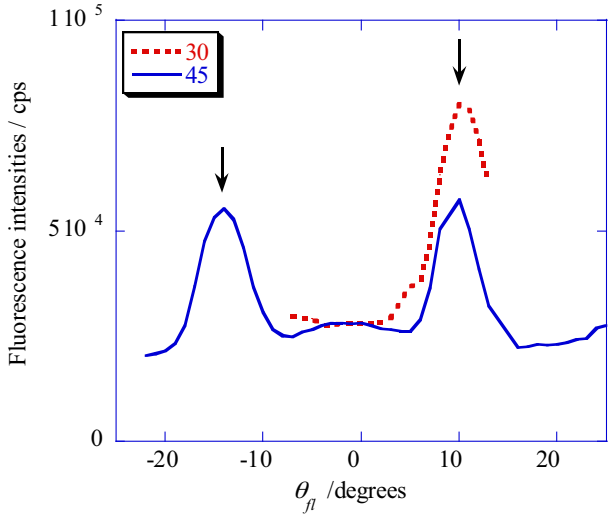

Fig. 4. Curves of fluorescence intensity against θ_{fl}. Incident angles were fixed at 30° (red dot) and 45° (blue solid). (For interpretation of the references to color in this figure legend, the reader is referred to the web version of this article.)

Fig. 5(a) and (b) shows the curves of fluorescence for Nos. 1 and 2 of 1D substrates measured against θ_{fl} under a fixed incident angle of 8° and 6°, respectively, corresponding to the resonance angle. In Fig. 5(a), the fluorescence peaks were found at 13°, while the maximum values were 2.7×10^5 cps. For No. 2 plasmonic chip shown in Fig. 5(b), the peak was not found in the detection range of 12–54°, because the reverse coupling angle is 10° outside the θ_{fl}-scanning range. (A scanning limit of the photomultiplier is $\theta_i + \theta_{fl} = 18°$ in our SPR-SPFS setup, therefore, under θ_i set to 6°, θ_{fl} can scan from 12°.) At its peak, fluorescence intensity is expected to be more than 4×10^5 cps, or more than four times greater than the peak value obtained in Fig. 3(b), 1×10^5 cps, detected with photomultiplier set at 55°. The peak values shown in Figs. 5(a) and (b) corresponds to 77 times and more than 110 times-enhanced fluorescence intensities compared with that detected on glass slides, respectively. Such large enhancements are considered to be due to the contribution of both the enhanced excitation field produced by GC-SPR and the enhanced emission by reverse coupling. The differences in the peak fluorescence intensity between Nos. 1 and 2 chips is considered to be due to the coupling efficiency with light caused by the differences in grating surface profile, including groove depth and duty ratio [13,14].

3.3. SPF under the substrate rotation for axis normal to surface

In the microscopic observation, the illumination light and fluorescence are concentrated by the objective lens through which the light comes in and out at various angles, designated by ψ, the light is non-polarized, and the irradiation angle and detection angle are limited by NA. Therefore, it is important that we examine the coupling conditions under rotation against substrate normal. Fig. 6(a) and (b) shows the curves of fluorescence intensity against incident angle and detection angle, respectively, for rotational No. 1 of 1D

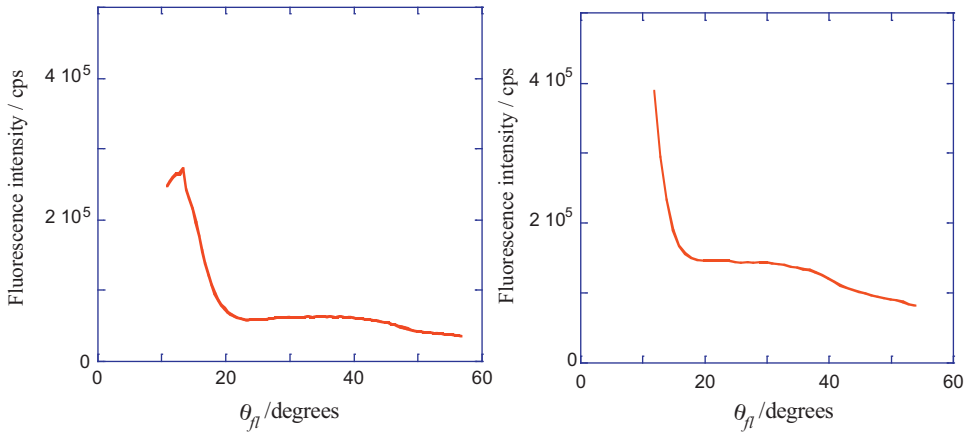

Fig. 5. Fluorescence intensities against detection angles. Incident angles were fixed at resonance angles of (a) 8° and (b) 6°, for gratings Nos. 1 and 2, respectively.

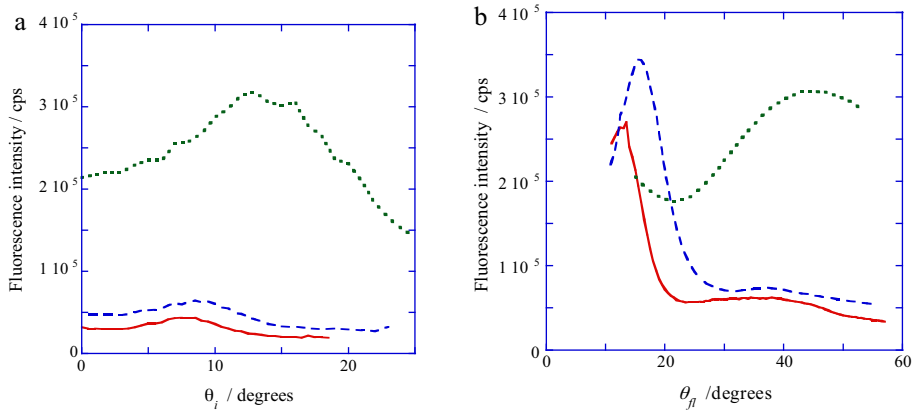

Fig. 6. Fluorescence intensity against (a) incident angle and (b) detection angle for $\psi = 0°$ (red solid), 30° (blue broken), and 55° (green dot); (a) detection angle fixed at 55°; (b) incident angle fixed at 8°, 9°, and 12° for $\psi = 0°$, 30°, and 55°, respectively. (For interpretation of the references to color in this figure legend, the reader is referred to the web version of this article.)

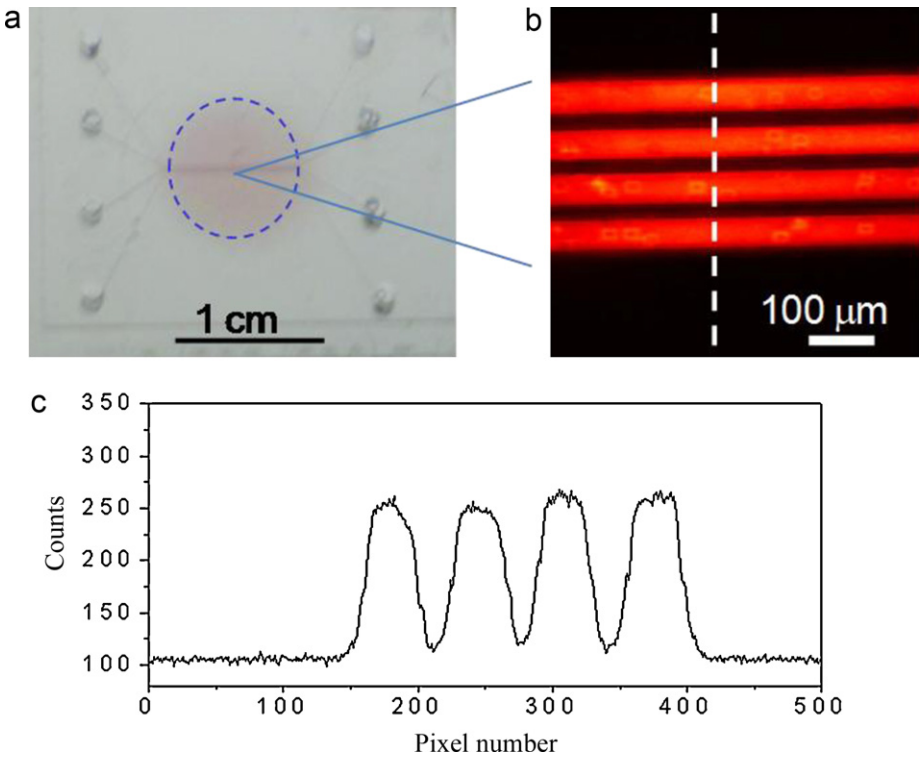

Fig. 7. (a) Photographic image of four microfluidic channels on a plasmonic substrate. The nanohole array area is indicated by a blue circle with a diameter of 9 mm. (b) Fluorescence microscopic image of four channels with the same concentration of Cy5-SA. (c) Cross-section plot along white dashed line in (b).

chip. As shown in Fig. 6(a), the peaks were found to be at 8°, 9°, and 12°, corresponding to the GC-SPR angles, for ψ of 0°, 30°, and 55°, respectively. The shift of resonance angle in response to substrate rotation was caused by the variation in coupling conditions. At rotational angle ψ above 60°, no more GC-SPR dip was found because of the limit on coupling conditions.

As shown in Fig. 6(a), the fluorescence intensity observed at peak angle for $\psi = 55°$ was markedly elevated. The reason could be interpreted from the results of the detection angle-scanning measurement shown in Fig. 6(b). Two of the fluorescence peaks other than for $\psi = 55°$ shown in Fig. 6(b) were very much (4–5 times) greater than the fluorescence enhanced only by the GC-SPR field shown in Fig. 6(a). In detection angle-scanning fluorescence measurement, unlike in incident angle-scanning measurement at the fixed angle of 55° for beam-line, the enhanced excitation field produced by GC-SPR and the enhanced emission by reverse coupling may contribute to detection of enhanced fluorescence. The reverse coupling angle θ_{fl} was 13°, 17°, and 44°, when ψ was set to 0°, 30°, and 55°, respectively. In the incident angle-scanning fluorescence measurement, the photomultiplier was fixed at 55° and the detection angle corresponds to the 43° when the incident angle comes to the resonance angle of 12°. It means that the incident angle-dependent fluorescence enhanced by the reverse coupling mode was therefore monitored at 55° of ψ and greater fluorescence intensity was observed than with ψ of 0° and 30° (Fig. 6(a)).

The resonance angles for all the ψ angles were included in the range of 8–12° and did not overlap with the range of reverse coupling angles of 13–44° in this plasmonic substrate with a pitch of 400 nm. In the 2D nanohole array with 400 nm-pitch, because of the symmetrical structure for 45° of ψ, the resonance angles were observed at 8–12° for any ψ. The reverse coupling angles were also observed at 13° for 0 and 90° of ψ and at 17° for $\psi = 30°$ and 60°.

3.4. Enhanced fluorescence detection in microfluidic channels

In the microscopic observation using objective lens with NA of 0.3, the ranges of irradiation angles and the detection angles cover 0–17°. It means that the ranges include the resonance angles for any rotational angle, ψ, and the reverse coupling angles for $\psi = 0–30°$ and 60–90° in 2D plasmonic substrate. This objective lens can provide the efficient coupling of irradiation light and the efficient detection of directional fluorescence.

PDMS four well-sealed micro channels were formed on the 2D biotinylated plasmonic substrates as shown in Fig. 7(a). As shown in Fig. 7(b) and (c), the same concentration detections showed almost the same fluorescence response, which indicates the homogeneous surface properties of the plasmonic substrate. This macroscopically homogeneous fluorescence enhancement on the surface will be important for Lab-on-a-chip applications.

To illustrate the enhancement effect of the 2D plasmonic substrate, we performed a concentration series analysis on both plasmonic and glass substrates, as shown in Fig. 8. An identical protocol for the bioanalysis of Cy5-SA was performed on both substrates. The results showed that the plasmonic substrate produces a significant enhancement of fluorescence biomolecular detection. Under the same conditions of illumination and detection, the fluorescence signal intensity on the plasmonic substrate was greatly enhanced compared to that on the glass slide, while the noise intensity only increased slightly (less than 20%) (Fig. 8(a) and (b)). Signal-to-noise ratio (SNR) is defined as the net channel intensity divided by the noise intensity and represents how easily a channel can be differentiated from noise. The SNR enhancement factors under concentrations of 1000, 100, 10, and 1 nM were calculated to be 13.5×, 16.4×, 14.5×, and 12.1×, respectively, which are greater than the 3.5× and 8.0× reported in a photonic crystal substrate [35]. The plasmonic substrate demonstrated 26.3× fluorescence enhancement compared with fluorescence intensity

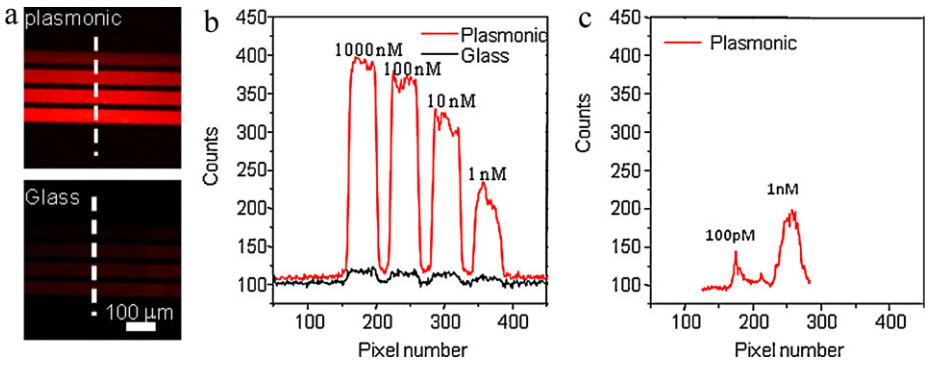

Fig. 8. (a) Fluorescence microscopic images of plasmonic and glass substrates with different concentrations of Cy5-SA: 1, 10, 100, and 1000 nM, from top to bottom. (b) Cross-section plot along white dashed line in (a). (c) The signals of 100 pM and 1 nM on the microfluidic channels of plasmonic substrate.

on the biotinylated glass slide at 100 nM. The enhancement factor of 26.3× is lower than that shown in our previous paper (100×), because the duty ratio is different between the plasmonic chips used here and previously. We note that both the SNR and enhancement values observed in microfluidic channels are lower than those we observed in the angular scanning measurement results. This is mainly attributable to the fact that light illuminates the samples not only from the resonance angle, but also from other angles that do not excite the highest enhancement. In other words, we observed an average enhanced effect under the microscope; in angular scanning measurement, however, the enhancement factor is always calculated from the highest enhancement at the resonance angle.

The limit of detection (LOD) is determined as three standard deviations above the background and is *ca.* 100 pM (Fig. 8(c)), which is at least one order of magnitude lower than the LOD on glass under the same measurement conditions. The LOD of 100 pM is considered to be reliable under the same condition, considering that the fluorescence intensity in channels observed with microscope is reproduced within error of ±5%. The amount of nonspecific adsorption to the PDMS microfluidics was not different between plasmonic chips and glass slides. Therefore, the difference in LOD was due to the enhanced fluorescence and the plasmonic chips were conveniently applicable to the biosensing.

4. Conclusion

Whereas most of surface plasmon-coupled fluorescence based on the reverse coupling mode is most often studied under the Kretschmann configuration, we demonstrated the reverse coupling mode in a grating-coupled emission. In our experiment using the grating substrates with 400-nm pitch and laser light with 632.8-nm wavelength, the reverse coupling angle was found to be 4–8° larger than the GC-SPR angle, which almost agrees with the angle estimated from the dispersion relationship. In sensing of proteins, fluorescence detected on our plasmonic chip was enhanced more than 110 times compared with that on glass slides. This higher sensitivity offers great advantages in application to new rapid and simple biosensor systems including a detection system of antigen-antibody interactions under the sandwich assay using labeled second antibodies.

Under a microscopic imaging using reverse coupling mode, a 2D plasmonic nanohole array substrate was developed for enhanced fluorescence detection of Cy5-SA using microfluidic channel devices. A fluorescence microfluidic bioanalysis found that the plasmonic substrate demonstrated 26.3× fluorescence enhancement at 100 nM and the lower detection limit (100 pM) compared to a glass slide with identical surface chemistry. This macroscopically homogeneous fluorescence enhancing plasmonic substrate will be invaluable for colorimetric detection in Lab-on-a-chip applications such as microfluidic ELISA device, and portable microarray biosensing.

Acknowledgements

The present study was supported by KAKENHI (Grant-in-Aid for Scientific Research) No. 19049016 on Priority Areas “Strong Photon-Molecule Coupling Fields (No. 470)” from the Ministry of Education, Culture, Sports, Science and Technology of Japan. We thank Ms. Akane Tanaka and Mr. Yoshiki Yokota for assistance with our experiments and thank Mr. Takashi Irie for his help in fabricating the microfluidic device.

References

[1] H. Raether, Surface Plasmons on Smooth and Rough Surfaces and on Gratings, Springer-Verlag, Heidelberg, 1988.
[2] A. Otto, in: B.O. Seraphin (Ed.), Optical Properties of Solids: New Developments, North-Holland Publishing Company, 1976, p. 677.
[3] W. Knoll, Annu. Rev. Phys. Chem. 49 (1998) 569.
[4] E. Popov, L. Tsonev, D. Maystre, Appl. Opt. 33 (1994) 5214.
[5] E. Popov, N. Bonod, S. Enoch, Opt. Express 15 (2007) 4224.
[6] T. Liebermann, W. Knoll, Colloids Surf. A 177 (2000) 115.
[7] K. Tawa, W. Knoll, Nucleic Acids Res. 32 (2004) 2372.
[8] S. Wedge, W.L. Barnes, Opt. Express 12 (2004) 3673–3685.
[9] N.F. Chiu, C. Yu, S.-Y. Nien, J.-H. Lee, C.-H. Kuan, K.-C. Wu, C.-K. Lee, C.-W. Lin, Opt. Express 15 (2007) 11608.
[10] Y.-J. Hung, I.I. Smolyaninov, C.C. Davis, H.-C. Wu, Opt. Express 14 (2006) 10825.
[11] K. Tawa, H. Hori, K. Kintaka, K. Kiyosue, Y. Tatsu, J. Nishii, Opt. Express 16 (2008) 9781.
[12] H. Hori, K. Tawa, Y. Tatsu, K. Kintaka, J. Nishii, Opt. Rev. 16 (2009) 216.
[13] X. Cui, K. Tawa, H. Hori, J. Nishii, Appl. Phys. Lett. 95 (2009) 133117.
[14] X. Cui, K. Tawa, H. Hori, J. Nishii, Adv. Funct. Mater. 20 (2010) 546.
[15] E. Matveeva, Z. Gryczynski, I. Gryczynski, J.R. Lakowicz, J. Immunol. Methods 286 (2004) 133.
[16] J. Malicka, I. Gryczynski, Z. Gryczynski, J.R. Lakowicz, Anal. Chem. 75 (2003) 6629.
[17] G. Winter, W.L. Barnes, Appl. Phys. Lett. 88 (2006) 051109.
[18] J. Feng, T. Okamoto, S. Kawata, Appl. Phys. Lett. 87 (2005) 241109.
[19] M.A. Burns, B.N. Johnson, S.N. Brahmasandra, K. Handique, J.R. Webster, M. Krishnan, T.S. Sammarco, P.M. Man, D. Jones, D. Heldsinger, C.H. Mastrangelo, D.T. Burke, Science 282 (1998) 484.
[20] R. Pal, M. Yang, R. Lin, B.N. Johnson, N. Srivastava, S.Z. Razzacki, K.J. Chomistek, D.C. Heldsinger, R.M. Haque, V.M. Ugaz, P.K. Thwar, Z. Chen, K. Alfano, M.B. Yim, M. Krishnan, A.O. Fuller, R.G. Larson, D.T. Burke, M.A. Burns, Lab Chip 5 (2005) 1024.
[21] L. Panga, G.M. Hwang, B. Slutsky, Y. Fainman, Appl. Phys. Lett. 91 (2007) 123112.
[22] L. Malic, T. Veres, M. Tabrizian, Biosens. Bioelectron. 26 (2011) 2053.
[23] B. Kuswandi, Nuriman, J. Huskens, W. Verboom, Anal. Chim. Acta 601 (2007) 141.
[24] E. Eteshola, M. Balberg, Biomed. Microdevices 6 (2004) 7.
[25] M. Hermann, T. Veres, M. Tabrizian, Anal. Chem. 80 (2008) 5160.
[26] M. Herrmann, T. Veres, M. Tabrizian, Lab Chip 6 (2006) 555.
[27] A.R. Abate, D. Lee, T. Do, C. Holtze, D.A. Weitz, Lab Chip 8 (2008) 516.

[28] D.A. Mair, M. Rolandi, M. Snauko, R. Noroski, F. Svec, J.M. Frechet, J. Anal. Chem. 79 (2007) 5097.
[29] K. Pitchaimani, B.C. Sapp, A. Winter, A. Gispanski, T. Nishida, Z.H. Fan, Lab Chip 9 (2009) 3082.
[30] L. Yu, C.M. Li, Y.S. Liu, J. Gao, W. Wang, Y. Gan, Lab Chip 9 (2009) 1243.
[31] L. Yu, Y.S. Liu, Y. Gan, C.M. Li, Biosens. Bioelectron. 24 (2009) 2997.
[32] L. Yu, C.M. Li, Q. Zhou, J.H.T. Luong, Bioconjug. Chem. 18 (2007) 281.
[33] L. Yu, C.M. Li, Q. Zhou, Front. Biosci. 10 (2005) 2848.
[34] E. Fort, S. Gresillon, J. Phys. D: Appl. Phys. 41 (2008) 0313001.
[35] P.C. Mathias, N. Ganesh, B.T. Cunningham, Anal. Chem. 80 (2008) 9013.
[36] K. Kintaka, J. Nishii, A. Mizutani, H. Kikuta, H. Nakano, Opt. Lett. 26 (2001) 1642.